Lyotropic Liquid Crystals as Nanoreactors for Nanoparticle Synthesis

Timothy M. Dellinger and Paul V. Braun*

Department of Materials Science & Engineering, Fredrick Seitz Materials Research Laboratory, and Beckman Institute for Advanced Science and Technology, University of Illinois at Urbana-Champaign, 1304 West Green Street, Urbana, Illinois 61801

Received September 25, 2003. Revised Manuscript Received March 2, 2004

A new methodology for the synthesis of nanoparticles using lyotropic liquid crystals as nanoreactors has been developed. The hydrophilic and hydrophobic domains of lyotropic phases have characteristic dimensions of 2−10 nm and thus can be used to confine reactants that are selectively soluble in only one domain to nanoscopic dimensions. Here, synthesis of Bi (a metal) and PbS (a compound semiconductor) nanoparticles is driven by bringing together reactants via the shear mixing of two liquid crystals, each containing dissolved reactants that are selectively soluble in one of the two phases, as proof-of-principle for this method. Modulating the phase of the lyotropic liquid crystals allows control over the geometry and interconnectivity of the nanoreactors, giving control over the diameter of nanoparticles produced. Decreasing concentration of precursors is shown to decrease particle size. It is also demonstrated that the nanoparticles produced are not agglomerated in the lyotropic liquid crystal during synthesis. The synthesized nanoparticles are characterized with TEM, electron diffraction, EDAX, and UV−Vis−NIR spectroscopy.

Introduction

Development of synthetic methodologies for the creation of nanoparticles of controlled size is currently a very active topic of research. Methodologies for bulk synthesis of nanoparticles generally utilize four basic strategies: condensation from a very dilute solution or gas,[1] solution-based surface passivation to arrest the growth of particles,[2,3] the use of physical confinement on a nanometer scale to constrain growth,[4] or nanometer-scale chemical confinement to limit the amount of material available for reaction.[5]

Lyotropic liquid crystals are made by mixing water with amphiphiles, which are molecules with connected hydrophobic blocks and hydrophilic blocks. When mixed with water, the hydrophobic blocks cluster together, as they are insoluble in water, and the hydrophilic blocks dissolve in the water. Because the hydrophobic and hydrophilic blocks are covalently linked, microphase separation does not occur, but the result is rather structures with characteristic dimensions on the order of 2−10 nm.[6] The packing geometry of the two portions of the amphiphile, along with the water-to-amphiphile ratio, determines the phase of the resulting liquid crystal. As shown schematically in Figure 1, for the oligo(ethylene oxide)$_{\overline{10}}$ oleyl ether/water system,[7,8] increasing the amphiphile:water ratio from 50:50 to 78:22 produces a phase change from hexagonal long-range periodicity to lamellar periodicity. Additionally, a nonpolar solvent can be added, which will be incorporated into the nonpolar domains. If sufficient nonpolar solvent is added, the hydrophobic portion becomes the majority component, and an inverse hexagonal phase is formed (Figure 1c).

The hydrophilic and hydrophobic domains of lyotropic liquid crystals have dimensions on the order of nanometers, so chemistries designed to operate exclusively in one domain of the liquid crystal are effectively constrained inside "nanoreactors". By controlling the liquid-crystalline phase, it is thus possible to control the size, shape, connectivity, and dimensionality of these nanoreactors, and thereby control the size and potentially the shape of nanoparticles grown inside them. For instance, altering the liquid-crystalline phase from hexagonal to lamellar to inverse hexagonal changes the geometry of the aqueous domains from three-dimensional continuous nanoreactors to sheetlike two-dimensional nanoreactors to rodlike one-dimensional nanoreactors as shown in Figure 1.

Previous work on the synthesis of nanoparticles in lyotropic liquid crystals includes the use of functional groups of the liquid crystal as reactants, the use of time delay chemistry, and the diffusion of reactants into the

* To whom correspondence should be addressed. E-mail: pbraun@uiuc.edu.

(1) Siegel, R. W.; Ramasamy, S.; Hahn, H.; Li, Z. Q.; Lu, T.; Gronsky, R. *J. Mater. Res.* **1988**, *3*, 1367−1372.
(2) Guzelian, A. A.; Banin, U.; Kadavanich, A. V.; Peng, X.; Alivisatos, A. P. *Appl. Phys. Lett.* **1996**, *69*, 1432−1434.
(3) Murray, C. B.; Norris, D. J.; Bawendi, M. G. *J. Am. Chem. Soc.* **1993**, *115*, 8706−8715.
(4) Hendershot, D. G.; Gaskill, D. K.; Justus, B. L.; Fatemi, M.; Berry, A. D. *Appl. Phys. Lett.* **1993**, *63*, 3324−3326.
(5) Watzke, H. J.; Fendler, J. H. *J. Phys. Chem.* **1987**, *91*, 854−861.
(6) Laughlin, R. G. *The Aqueous Phase Behaviour of Surfactants*; Academic Press Inc.: San Diego, 1994.
(7) Kunieda, H.; Shigeta, K.; Ozawa, K.; Suzuki, M. *J. Phys. Chem. B* **1997**, *101*, 7952−7957.
(8) Braun, P. V.; Osenar, P.; Tohver, V.; Kennedy, S. B.; Stupp, S. I. *J. Am. Chem. Soc.* **1999**, *121*, 7302−7309.

10.1021/cm0349194 CCC: $27.50
Published on Web 05/01/2004

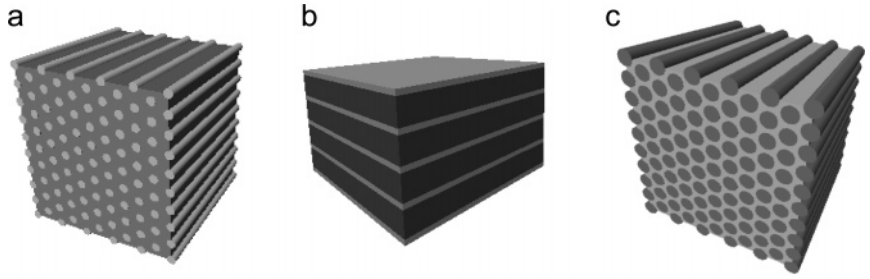

Figure 1. Schematics of the lyotropic liquid crystals used in this study, depicting periodically ordered hydrophilic and hydrophobic domains: (a) hexagonal phase, (b) lamellar phase, and (c) inverse hexagonal phase. Hydrophilic domains are dark-colored; hydrophobic domains are light-colored.

liquid crystal from solution. Puvvada et al.[9] and Qi et al.[10] have used surfactants as reducing agents, producing Pd nanoparticles in a bicontinuous cubic phase and Ag nanoparticles in a lamellar phase. O'Sullivan et al.[11] used water as a hydrolysis agent to synthesize β-FeOOH at elevated temperatures in a lamellar phase. The addition of thioacetamide to a liquid crystal, which will decompose to produce H_2S on time scales longer than the time required for liquid crystals to order, has been used by Li et al.[12] to produce CdS nanowires in hexagonal and lamellar phases and by Zhang et al.[13] to produce ZnS nanorods in a lamellar phase. Ding et al.[14] have used H_2 gas as a reducing agent for the synthesis of Pd/polymer composites via diffusion into a cross-linked inverse hexagonal phase. Three-dimensional diffusion of ionic reactants is possible by restricting syntheses to phases with percolating hydrophilic regions: Yang et al.[15] used Na_2S diffusing into a percolated bicontinuous phase containing $Pb(NO_3)_2$ to synthesize PbS nanoparticles. Additional uses of lyotropic liquid crystals as a reactor environment include the use of H_2S infusion,[8,16] the incorporation of macroscopic (>3 mm) solid reactants,[17] or electrochemistry,[18,19] all of which produce templated replicas of the phase used.

The use of time delay chemistry, the use of the components of the liquid crystal as reactants, and the use of diffusible reactants impose restrictions on the chemistries that can be used and thus on the types of nanoparticles that can be produced. The shear mixing synthetic strategies presented here do not rely on specific interactions between the precursors and the liquid crystal, but rather are general and can be adapted to a wide range of nanoparticle syntheses. Any material that can be made by bringing together two solutions can in principle use the methodology presented here without having to adapt the synthetic pathway and the liquid crystal to each other. In this paper, we will specifically focus on two materials systems: bismuth (a metal) and lead sulfide (a compound semiconductor) as proof-of-principle.

Routes to bismuth nanoparticles in particular have been of interest[20−23] due to theoretical predictions of enhanced thermoelectric properties in nanosized bismuth.[24,25] Nanosized bismuth, however, has proven to be difficult to synthesize because there are no known capping or stabilization agents analogous to thiols on gold, and reported syntheses use stabilization agents that are metastable. Due to the low effective mass of the charge carriers, bismuth nanoparticles begin to exhibit quantum confinement at the unusually large diameter of ~50 nm, undergoing a semimetal to semiconductor transition as nanoparticle size decreases. The intrinsic low thermal conductivity of bismuth, coupled with the narrow band gap afforded by quantum confinement, makes nanosized bismuth an ideal material for thermoelectric applications.

PbS is a compound semiconductor that exhibits quantum confinement effects with decreasing particle size. There is an increase in the size of the band gap for smaller particles, and the optical absorption edge is strongly blue-shifted, moving from ~3200 nm in the bulk to ~700 nm for 2.5-nm diameter particles.[26] PbS is commonly synthesized by reaction of a lead salt with either H_2S or Na_2S.

Here, we demonstrate the use of hexagonal, lamellar, and inverse hexagonal lyotropic liquid crystals based on the nonionic amphiphile oligo(ethylene oxide)$_{\overline{10}}$ oleyl ether as generalized synthetic nanoreactors for the creation of metal and compound semiconductor nanoparticles through shear mixing.

Experimental Section

All chemicals were used as-received from Acros unless otherwise indicated. Due to the air sensitivity of bismuth

(9) Puvvada, S.; Baral, S.; Chow, G. M.; Qadri, S. B.; Ratna, B. R. *J. Am. Chem. Soc.* **1994**, *116*, 2135−2136.
(10) Qi, L.; Gao, Y.; Ma, J. *Colloids Surf. A* **1999**, *157*, 285−294.
(11) O'Sullivan, E. C.; Ward, A. J. I.; Budd, T. *Langmuir* **1994**, *10*, 2985−2992.
(12) Li, Y.; Wan, J.; Gu, Z. *Mater. Sci. Eng. A* **2000**, *286*, 106−109.
(13) Zhang, D.; Qi, L.; Cheng, H.; Ma, J. *J. Colloid Interface Sci.* **2002**, *246*, 413−416.
(14) Ding, J. H.; Gin, D. L. *Chem. Mater.* **2000**, *12*, 22−24.
(15) Yang, J. P.; Qaqri, S. B.; Ratna, B. R. *J. Phys. Chem.* **1996**, *100*, 17255−17259.
(16) Braun, P. V.; Osenar, P.; Stupp, S. I. *Nature* **1996**, *380*, 325−328.
(17) Attard, G. S.; Goltner, C. G.; Corker, J. M.; Henke, S.; Templer, R. H. *Angew. Chem., Int. Ed. Engl.* **1997**, *36*, 1315−1317.
(18) Attard, G. S.; Bartlett, P. N.; Coleman, N. R. B.; Elliott, J. M.; Owen, J. R.; Wang, J. H. *Science* **1997**, *278*, 838−840.
(19) Bartlett, P. N.; Birkin, P. N.; Ghanem, M. A.; Groot, P. d.; Sawicki, M. *J. Electrochem. Soc.* **2001**, *148*, C119−C123.
(20) Fang, J.; Stokes, K. L.; Wiemann, J.; Zhou, W. *Mater. Lett.* **2000**, *42*, 113−120.
(21) Foos, E. E.; Stroud, R. M.; Berry, A. D.; Snow, A. R.; Armistead, J. P. *J. Am. Chem. Soc.* **2000**, *122*, 7114−7115.
(22) Fang, J.; Stokes, K. L.; Wiemann, J. A.; Zhou, W. L.; Dai, J.; Chen, F.; O'Connor, C. J. *Mater. Sci. Eng. B* **2001**, *83*, 254−257.
(23) Fang, J. Y.; Stokes, K. L.; Zhou, W. L. L.; Wang, W. D.; Lin, J. *Chem. Commun.* **2001**, *18*, 1872−1873.
(24) Dresselhaus, M. S.; Lin, Y.-M.; Cronin, S. B.; Rabin, O.; Black, M. R.; Dresselhaus, G.; Koga, T. In *Recent Trends in Thermoelectric Materials III*; Tritt, T. M., Ed.; Academic Press: San Diego, CA, 2001; Vol. 71, pp 1−121.
(25) Dresselhaus, M. S.; Dresselhaus, G.; Sun, X.; Zang, Z.; Cronin, S. B.; Koga, T.; Ying, J. Y.; Chen, G. *Microscale Thermophys. Eng.* **1999**, *3*, 89−100.
(26) Wang, Y.; Suna, A.; Mahler, W.; Kasowski, R. *J. Chem. Phys.* **1987**, *87*, 7315−7322.

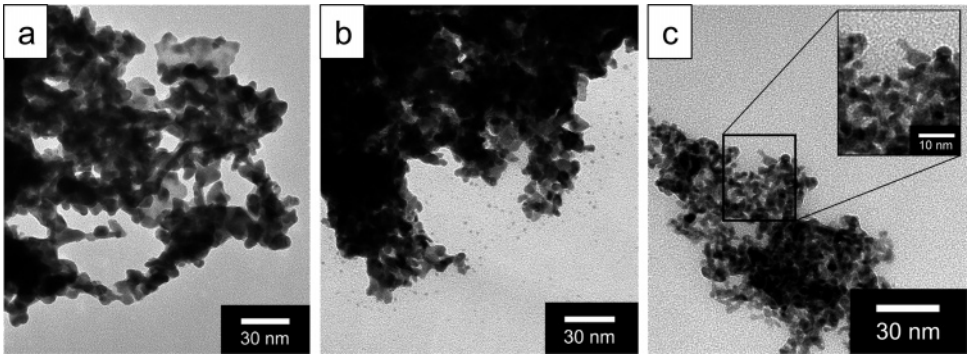

Figure 2. TEM micrographs of Bi nanoparticles produced by shear-mixing lyotropic liquid crystals containing 0.05 M $BiCl_3$ and 0.4 M $CrCl_2$ as the aqueous component. (a) Hexagonal phase, (b) lamellar phase, and (c) inverse hexagonal phase.

nanoparticles to oxidation, Bi nanoparticle synthesis was performed in an Ar-filled glovebox or using standard Schlenk line techniques under N_2. In a typical synthesis, 0.01 M $BiCl_3$ (Sigma-Aldrich) in HCl (pH ~1.0) was drawn into a 3-mL disposable syringe, and oligo(ethylene oxide)$_{\overline{10}}$ oleyl ether (Sigma-Aldrich), warmed to its melting point (35 °C), was drawn into a second 3-mL disposable syringe. The syringes were then connected with a stainless steel union, with care taken not to introduce air bubbles, and by forcing the contents of the syringes back and forth at a rate of ~5 cm^3/s, the solution was shear-mixed, forming a liquid crystal, evidenced by an increase in viscosity and verified using polarized optical microscopy. A second liquid crystal was also made with an identical amphiphile: solution weight ratio, with the aqueous portion containing 0.4 M $CrCl_2$ (Acros), a powerful reducing agent. The syringes containing these two liquid crystals were connected and shear-mixed at ~5 cm^3/s for approximately 2 min, resulting in the formation of bismuth nanoparticles. Experiments were also performed using 0.05 M $BiOClO_4$ (Aldrich) instead of $BiCl_3$ + HCl. These experiments required that the amphiphile be washed to remove anions which would cause the precipitation of, for example, BiOCl. The amphiphile was washed three times in a separatory funnel with dichloromethane and water, with the dichloromethane fraction kept after each washing, as the amphiphile has greater solubility in the nonpolar phase. The amphiphile was then isolated by evaporating the CH_2Cl_2 under vacuum.

PbS nanoparticles were produced in a similar manner, using liquid crystals made with solutions of $Pb(NO_3)_2$ or $Pb(OAc)_2$ ($Pb(CH_3COO)_2$) (J. T. Baker Chemical Co.), ranging from 0.005 to 0.1 M, and a saturated solution of H_2S (nominally 0.1 M) produced by bubbling H_2S through water.

The capping agent sodium hexametaphosphate (Alfa Aesar) was used in some PbS experiments. Lead sulfide nanoparticles were prepared in these experiments by shear-mixing a lamellar liquid crystal containing 0.05 M $Pb(OAc)_2$ with a lamellar liquid crystal containing 0.05 M Na_2S, creating a liquid crystal which contained PbS nanoparticles. A third lamellar liquid crystal, containing 0.05 M sodium hexametaphosphate, was prepared, which was shear-mixed with the liquid crystal containing PbS. The nanoparticles were then washed with ethanol as described below.

Formulations (ratios by weight) for the liquid-crystalline phases used were hexagonal, 50:50 amphiphile:aqueous solution; lamellar, 78:22 amphiphile:aqueous solution; and inverse hexagonal, 48:12:40 amphiphile:aqueous solution:cyclohexane. Additionally, control experiments were performed using an isotropic 70:30 solution of 20 000 MW poly(ethylene glycol): water in order to reproduce the chemistry of the ordered aqueous domains of the lamellar liquid crystal. Control experiments in aqueous solutions of 10% amphiphile were also performed.

Workup was performed as follows: following nanoparticle synthesis, the liquid crystals were dissolved in ethanol, and the nanoparticles were removed by washing three times in ethanol using centrifugation. After sonication to disperse the particles, samples for electron microscopy were prepared by placing a drop of solution on a holey carbon TEM grid, and microscopy was performed using a Phillips CM 12 TEM. As expected, the particles agglomerated irreversibly when no capping agents were used. Energy-dispersive X-ray spectroscopy (EDAX), dark field microscopy, and electron diffraction were used to confirm that individual nanoparticles were single crystals of the expected composition and phase. Diffraction patterns matched JCPDF 44-1246 (Bismuth) and JCPDF 05-0592 (PbS). UV−Vis−NIR spectroscopy of the PbS nanoparticles was taken in transmission mode on samples of the liquid crystal immediately after synthesis using a Cary 5G UV−Vis−NIR spectrophotometer over the range of 300−2500 nm (4.13−0.50 eV). Samples of each liquid crystal were pressed between two glass slides, with either one or three 0.2-mm-thick glass cover slip spacers used to control the sample thickness. Liquid crystals of the same phase, containing only water, amphiphile, and, for the inverse hexagonal phase, cyclohexane, were used as reference samples.

Results and Discussion

Bi Nanoparticle Synthesis. Shear mixing in the synthesis experiments presented here serves to connect, for example, the $BiCl_3$-containing aqueous domains with the $CrCl_2$-containing aqueous domains. Diffusion within these newly connected nanoreactors allows the reactants to come together, resulting in the formation of nanoparticles. The effect of liquid-crystalline phase on the diameter of the bismuth nanoparticles is shown in Figure 2. Dramatic reduction in particle size is found as the mesophase was varied from a hexagonal phase, which consists of three-dimensional hydrophilic domains, to a lamellar phase, which consists of two-dimensional sheetlike hydrophilic domains, to an inverse hexagonal phase, which consists of one-dimensional rodlike hydrophilic domains. Controlling the dimensionality of confinement serves to control ion transport within the nanoreactors. Constraining ion transport serves to create smaller particles, as fewer ions are able to reach a given growing particle.

Particles can be thought of as collections of all reactants which were originally within an effective diffusion distance of the particle. Reducing the dimensionality of the nanoreactors from three- to two- to one-dimensional reduces this volume of available material from a sphere to a disk to a line segment, as ion transport through the hydrophobic domains of the liquid crystal is essentially prohibited. This was confirmed through control experiments where two lamellar or inverse hexagonal liquid crystals are poured sequentially into a vial, but not mixed. Even after several days, chemical reactions were observed to occur only at a thin

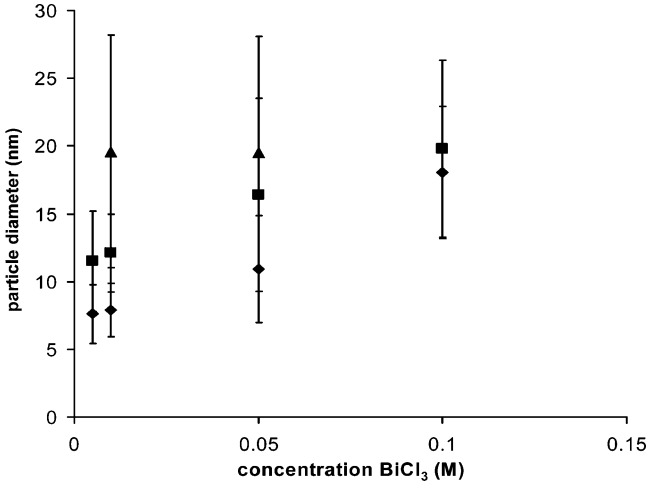

Figure 3. Average diameter of Bi nanoparticles synthesized in a hexagonal phase (triangles), lamellar phase (squares), and an inverse hexagonal phase (diamonds) vs concentration of $BiCl_3$, with concentration of $CrCl_3$ held constant at 0.4 M.

layer at the interface, confirming the inability of the Bi^{3+} and Cr^{2+} ions to cross the hydrophobic domains between the nonconnected two- and one-dimensional polar nanodomains of the lamellar and inverse hexagonal liquid crystals, respectively.

The average particle diameter of the Bi nanoparticles produced in the various liquid-crystalline phases is plotted in Figure 3 against the concentration of $BiCl_3$, with the concentration of $CrCl_2$ kept at 0.4 M. The data in Figure 3 were produced by averaging the major and minor axis of each particle in a representative cluster of at least 25 particles per data point, and the error bars represent one standard deviation. In contrast, the two sets of control experiments, the first using homogeneous aqueous solutions of poly(ethylene glycol) with no long-range order, and the second using 10% amphiphile and 90% aqueous solution, also with no long-range order, both produced polydisperse bismuth particles with sizes ranging from hundreds of nanometers to micrometers. The data indicate a strong trend that reducing the nanoreactor dimensionality reduces particle size, and that reducing the concentration of precursor salts available for reaction in any given nanoreactor reduces the particle size.

Four of the experiments presented in Figure 3 were repeated to confirm the reproducibility of the particle sizes and size distributions. Repeat experiments using 0.05 M $BiCl_3$ in lamellar and inverse hexagonal phases produced particles that were 17.6 ± 6.0 and 10.6 ± 2.4 nm, respectively. These sizes are comparable to the original experiments which produced particles 16.4 ± 7.1 nm (lamellar phase) and 10.9 ± 3.9 nm (inverse hexagonal phase). Repeat experiments using 0.005 M $BiCl_3$ in lamellar and inverse hexagonal phases produced particles that were 9.7 ± 2.1 and 6.9 ± 1.2 nm, likewise similar to the original experiments which produced particles 11.5 ± 3.7 nm (lamellar phase) and 7.6 ± 2.2 nm (inverse hexagonal phase).

One feature of lamellar liquid crystals is that lamellar spacing can be controlled by varying the amphiphile: water ratio.[8] The hydrophobic portion of the liquid crystal keeps the same dimensions, but the aqueous portion changes in thickness, thereby changing the size

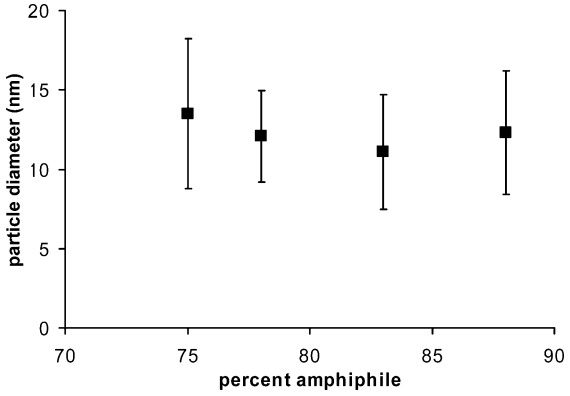

Figure 4. Average diameter of Bi nanoparticles synthesized in lamellar phases as a function of amphiphile content of the lamellar phase.

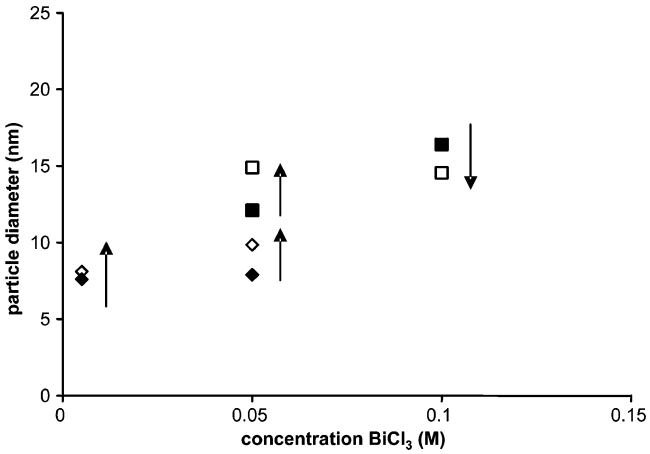

Figure 5. Average diameter of Bi nanoparticles synthesized in lamellar (squares) and inverse hexagonal (diamonds) phases. Open symbols are particles synthesized using 2 M $CrCl_2$; closed symbols are particles synthesized using 0.4 M $CrCl_2$.

of the nanoreactor. The diameters of bismuth nanoparticles synthesized in lamellar liquid crystals with varying lamellar spacings are shown in Figure 4. Nanoparticle size is only weakly dependent on lamellar spacing, if at all, confirming that size control of the nanoparticles comes not through a direct templating but rather through a control of precursor material available for reaction. Simply stated, variation of the thickness of the nanoreactors results in only a small change in the total size of the nanoreactor.

Increasing the concentration of reducing agent from 0.4 to 2.0 M $CrCl_2$ resulted in a slight increase in Bi nanoparticle diameter for particles synthesized in lamellar and inverse hexagonal phases, as seen in Figure 5, with the exception of the 0.1 M $BiCl_3$ lamellar experiment, where particle diameter decreased. An increase in reducing agent might be expected to decrease particle size since the greater concentration should result in faster reactions and thus less diffusion of reactants toward growing particles. For the lower concentrations of $BiCl_3$ (0.01 and 0.05 M), 0.4 M $CrCl_2$ is already an excess of reducing agent, being 13.3 and 2.6 times the amount required to reduce all of the $BiCl_3$, respectively. Since there is already a large excess of reducing agent, increasing concentration has little effect. The increase in concentration of reducing agent may reduce the liquid-crystalline order, which could increase the average particle size. For the 0.1 M $BiCl_3$ experiment, 0.4

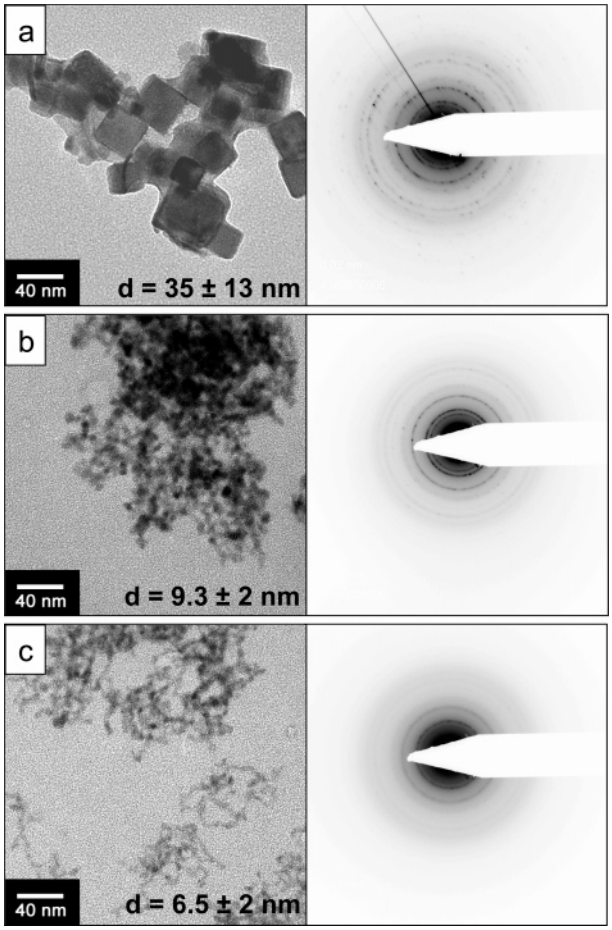

Figure 6. TEM micrographs (left) and selected area electron diffraction patterns (right) of PbS nanoparticles produced by shear mixing lyotropic liquid crystals containing 0.05 M $Pb(NO_3)_2$ and 0.1 M H_2S. (a) Hexagonal phase, (b) lamellar phase, and (c) inverse hexagonal phase.

M $CrCl_2$ is only 1.3 times the amount required for full reaction, and thus not surprisingly, an increase in the $CrCl_2$ concentration to 2.0 M (6.6 equiv) decreases particle size.

Shear-mixing experiments performed using 0.05 M $BiOClO_4$ instead of 0.05 M $BiCl_3$ as the Bi source in one liquid-crystalline phase and 0.4 M $CrCl_2$ as the reducing agent in the other liquid-crystalline phase produced smaller nanoparticles. In the lamellar phase, $BiOClO_4$ resulted in nanoparticles with an average particle diameter of 13.2 nm, as compared to 16.4 nm for $BiCl_3$ and in the inverse hexagonal phase 8.7 nm as compared to 10.9 nm for $BiCl_3$. The size dispersity also decreased upon changing the salt to $BiOClO_4$. The standard deviation in particle diameter decreased from 7.2 to 4.1 nm in the lamellar phase and from 3.9 to 2.6 nm in the inverse hexagonal phase. The observation that the $BiOClO_4$ precursor results in smaller nanoparticles than the $BiCl_3$ precursor was confirmed through a repeat of the nanoparticle synthesis from 0.05 M $BiOClO_4$ in the lamellar phase, which yielded 11.5 ± 2.1 nm nanoparticles. Unlike $BiCl_3$, $BiOClO_4$ does not require the addition of acid in order to be stable in aqueous solution. It may be that decreasing the quantity of dissolved species in the liquid crystal increases the liquid-crystalline order, thereby producing smaller particles with smaller size dispersity.

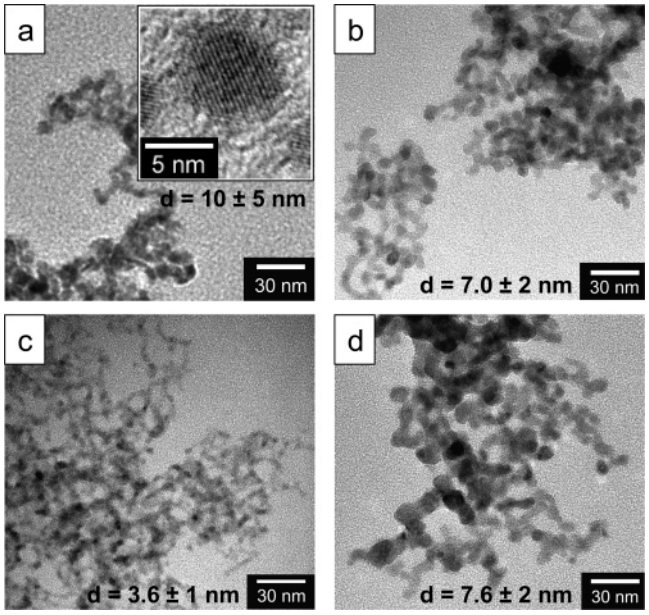

Figure 7. TEM micrographs of PbS nanoparticles produced by shear-mixing lyotropic liquid crystals containing 0.05 M $Pb(OAc)_2$ and 0.1 M H_2S: (a) hexagonal phase, (b) lamellar phase, and (c) inverse hexagonal phase. (d) PbS nanoparticles formed in unstructured PEO.

PbS Nanoparticle Synthesis. Figure 6 shows micrographs of PbS nanoparticles produced from lead nitrate via shear mixing in the hexagonal, lamellar, and inverse hexagonal phases. Particles produced in the hexagonal phase are somewhat polydisperse and exhibit the cubic morphology common for PbS. Similar to the bismuth metal case, a size reduction is seen in going to the lamellar and then the inverse hexagonal phases, and concurrently, the particles take on a spherical morphology. Selected-area electron diffraction reveals a high degree of crystallinity in the nanoparticles. Control experiments consisting of mixing 0.05 M $Pb(NO_3)_2$ and H_2S saturated water in aqueous solution and in PEO mixtures produced 31 ± 20 and 27 ± 12 nm cubic particles, respectively, from 0.05 M $Pb(NO_3)_2$. Likewise, control experiments using the same aqueous solutions plus 10% amphiphile produced 41 ± 21 nm particles.

Using lead acetate as the lead source instead of lead nitrate produces the particles presented in Figure 7. Interestingly, control experiments in unstructured liquids also generated small particles. Reacting 0.05 M $Pb(OAc)_2$ PEO mixtures with H_2S saturated water PEO mixtures generated 7.6 ± 2.2 nm particles, and mixing 0.1 M $Pb(OAc)_2$ aqueous solutions with H_2S saturated water resulted in particles that were 11.3 ± 5 nm. As a further control experiment, PbS was synthesized in a 10% amphiphile aqueous solution using, as the lead source, a mixture of 0.05 M $Pb(NO_3)_2$ and 0.1 M acetic acid, and H_2S saturated water as the sulfur source. The resulting particles were 48 ± 27 nm, ruling out the possibility that the acetate anion might be acting as a capping agent.

The difference in particle morphology between the two syntheses can be understood by considering the reaction byproducts. Synthesis of PbS from the $Pb(OAc)_2$ generates acetic acid (a weak acid, $pK_a = 4.8$), while synthesis from $Pb(NO_3)_2$ generates nitric acid (a strong acid, $pK_a = -1.3$). The strong acid has the possibility to initially

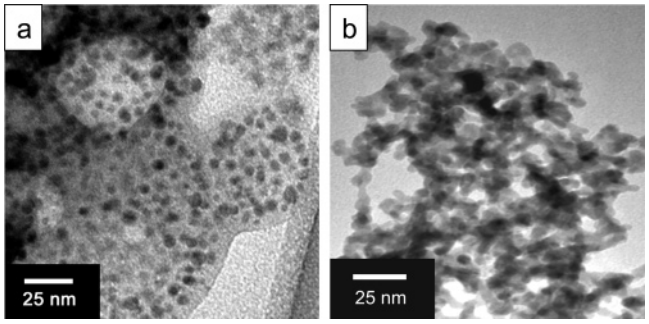

Figure 8. TEM micrograph of PbS nanoparticles produced from 0.05 $Pb(OAc)_2$ + 0.05 M Na_2S in a lamellar liquid crystal. (a) Particles stabilized after synthesis with sodium hexametaphosphate, demonstrating that particles are not aggregated during synthesis; (b) particles as synthesized.

dissolve growing PbS particles, at least until the H_2S concentration is locally high enough, thus making the reaction reversible and allowing the possibility of Ostwald ripening of particles. Acetic acid, on the other hand, does not dissolve PbS, and the reaction is not reversible, thus particle size is determined by the original diffusion of the precursors into particles. The irreversibility of the reaction explains why small nanoparticles are produced even in the unstructured control experiments. It remains consistent, in both the acetate and nitrate systems, that decreasing nanoreactor dimensionality reduces the average size of the nanoparticles produced.

Additionally, experiments in unstructured solutions of 10% amphiphile, using 0.1 M Na_2S as the sulfur source instead of H_2S, produced nanoparticles from both 0.05 M $Pb(NO_3)_2$ and 0.05 M $Pb(OAc)_2$, with particle sizes being 6.6 ± 0.8 and 7.5 ± 1.0 nm, respectively. Again, the explanation lies in the reaction byproducts: unlike nitric acid, neither sodium nitrate nor sodium acetate are strong acids with the ability to dissolve PbS, and thus growing particles could not undergo ripening.

It is interesting to consider whether the PbS nanoparticles are physically touching during the syntheses. An experiment was performed in which PbS nanoparticles were first synthesized without capping agent, but then before dissolving the liquid crystal, a separate liquid crystal containing sodium hexametaphosphate, a known capping agent for the II−VI semiconductor CdS,[27] and presumably PbS, was shear-mixed into the original synthesis. This generated the particles presented in Figure 8a. These can be compared with nanoparticles synthesized through an identical procedure without the addition of sodium hexametaphosphate, which are clearly aggregated in the TEM micrograph (Figure 8b). The individual PbS nanoparticles in Figure 8a are not in direct contact, but rather are separated by the sodium hexametaphosphate capping agent. Since it was possible to prevent agglomeration after the synthesis but before workup, this demonstrates that the nanoparticles aggregate during or after workup and are not agglomerated in the liquid crystal during synthesis.

As a further measure of nanoparticle size control, UV−Vis−NIR spectroscopy can be used to investigate

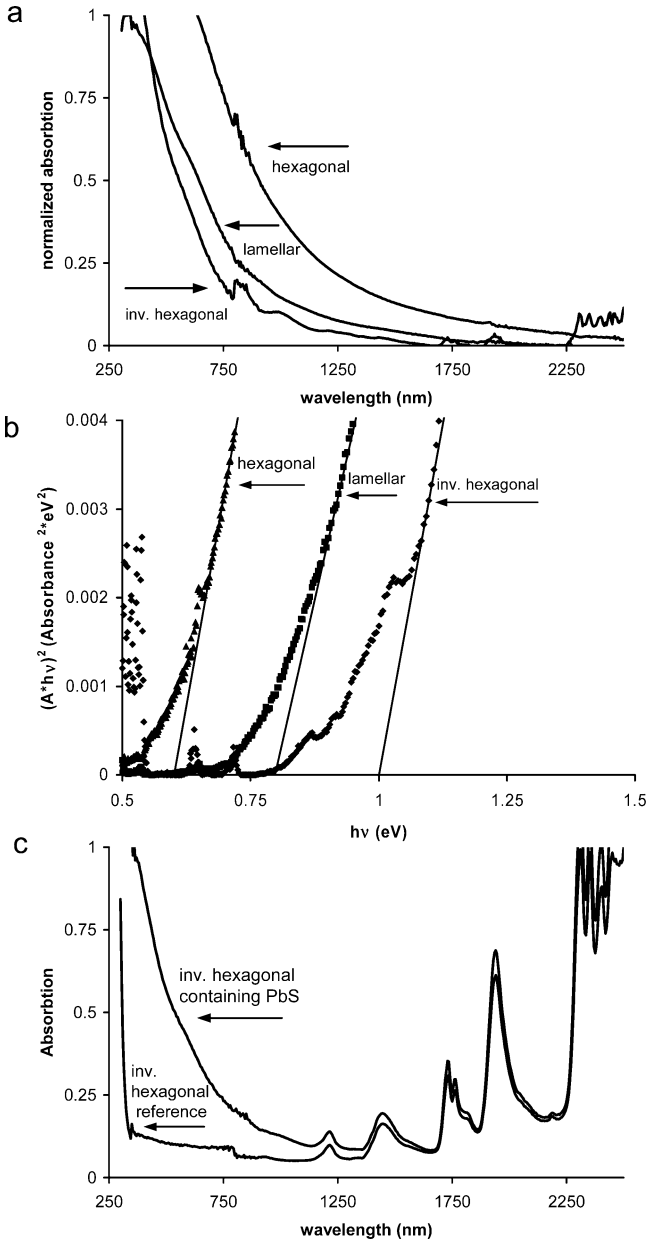

Figure 9. UV−Vis−NIR spectroscopy of PbS nanoparticles in the three liquid crystals synthesized from liquid crystals containing 0.05 M $Pb(NO_3)_2$ and 0.1 M H_2S. (a) Normalized absorbance vs wavelength, (b) plot of (absorbance * $h\nu$)^2 vs $h\nu$ in order to determine band gap, and (c) actual absorbance data for the PbS nanoparticle filled inverse hexagonal liquid crystal, and the reference liquid crystal containing no PbS or dissolved salts.

the increase in electronic band gap that is induced by quantum confinement as nanoparticle size decreases. UV−Vis−NIR spectra were recorded on the PbS nanoparticles while they were suspended in the liquid crystal by sandwiching a sample of the liquid crystal between glass slides, with either one or three 0.2-mm-thick glass cover slips used as spacers. Liquid crystals of the same phase, containing only water, amphiphile, and in the case of the inverse hexagonal phase, cyclohexane, were used as reference samples. The UV−Vis−NIR spectra of the nanoparticles synthesized from the nitrate salt are presented in Figure 9a. The spectrum of a sample obtained in the hexagonal phase is the absorbance of a 0.2-mm-thick sample of the PbS nanoparticles synthe-

(27) Ramsden, J. J.; Gratzel, M. *Faraday Trans.* **1984**, *80*, 919−933.

sized from 0.05 M $Pb(NO_3)_2$ + 0.1 M H_2S, dispersed in the hexagonal liquid crystal, after reference subtraction. The lamellar and inverse hexagonal samples contain a lower concentration of PbS per unit volume, and thus are normalized to represent the same concentration of PbS and path length as those of the hexagonal spectrum.

Plotting the data as (absorbance * $h\nu$)^2 vs $h\nu$, with $h\nu$ being the energy of the incident light in eV, is presented in Figure 9b. Extrapolation of the linear region of the curve to zero allows determination of the band gap of the nanoparticles,[26,28] with deviation from linear behavior expected to occur near the band gap. Although it is immediately clear from Figure 9b that the particles synthesized in the three different liquid-crystalline phases have markedly different band gaps, definitive fits to the data are not possible. The reasons that a clear linear fit is not evident include strong overlapping absorption bands from the liquid crystal, nanoparticle polydispersity, and scatter. For example, as presented in Figure 9c, prominent absorption bands exist in both the inverse hexagonal liquid crystal containing PbS nanoparticles and in the inverse hexagonal control sample, at 1210 and 1430 nm. These overlap strongly with the absorption edge of the PbS particles and make background subtraction somewhat difficult in these spectral regions.

With regard to nanoparticle polydispersity, a linear fit should only be expected from monodisperse particles. Deviations from linearity reveal that the nanoparticles are polydisperse; thus, the total spectrum is due to the contributions of particles with a range of band gaps. This is in agreement with the results of microscopy, which also reveal size polydispersity in the samples. Finally, light scatter by the particles or by the liquid crystal might also complicate the data analysis, but should not change the overall interpretation of the data. Even with these complications, the spectra reveal that nanoparticles produced in nanoreactors with decreased dimensionality have larger band gaps, and thus are smaller in size.

Effect of Shear. One possible concern with shear mixing of lyotropic liquid crystals is the potential disruption of the phase due to the shearing. Studies of the effect of shear on $(CH_2)_x-(OCH_2CH_2)_y$/water type lyotropic liquid crystals such as those used here show orientation effects with respect to the shear direction for $(CH_2)_{16}-(OCH_2CH_2)_6$-based systems depending on shear rate,[29,30] and a shear-induced transition from oriented lamellae to multilamellar vesicles (often termed "onions") for $(CH_2)_{12}-(OCH_2CH_2)_4$-based lyotropic liquid crystals.[31−33] Disruption of liquid-crystalline order has not been seen at any shear rate for these systems. We have estimated the shear rate in our system to be ∼2500 s^{-1}, which falls in a regime that exhibits a mixture of two orientations for $(CH_2)_{16}-(OCH_2CH_2)_6$ and a regime of multilamellar vesicles for $(CH_2)_{12}-(OCH_2CH_2)_4$, and thus we do not believe that phase disruption is occurring during shear mixing.

Conclusions

We have demonstrated a novel and general methodology for the synthesis of nanoparticles based on reactions in nanoreactors formed by lyotropic liquid crystals. Since nanoparticle synthesis in nonionic lyotropic liquid crystals does not rely on specific interactions between the amphiphile and the reactants or products of the chemical reaction, the amphiphile chemistry need not be custom-designed to the chemistry of the nanoparticles. We have demonstrated it is possible to perform chemical reactions within the nanodomain space of lyotropic liquid crystals to produce metallic, semiconducting, and potentially oxide nanoparticles and that the size of the nanoparticle produced can be modulated by varying the connectivity of the nanoreactors by varying the phase of the liquid crystal. The synthetic methodology described here also allows for inclusion of stabilizing agents either during or after nanoparticle synthesis, which can prevent agglomeration of the nanoparticles.

Acknowledgment. This material is based in part upon work supported by the U.S. Department of Energy, Division of Materials Sciences, under Award No. DEFG02-ER9645439, through the Frederick Seitz Materials Research Laboratory at the University of Illinois at Urbana-Champaign, and by the National Science Foundation NSEC DMR-0117792 at the University of Illinois at Urbana−Champaign. UV−Vis−NIR transmission spectra were obtained in the Laser and Spectroscopy Facility at the Frederick Seitz Materials Research Laboratory. Electron microscopy was carried out in the Center for Microanalysis of Materials, University of Illinois, which is partially supported by the U.S. Department of Energy under Grant DEFG02-91-ER45439.

CM0349194

(28) Bube, R. H. *Electronic Properties of Crystalline Solids*; Academic Press: New York, 1974.
(29) Penfold, J.; Staples, E.; Tucker, I.; Tiddy, G. J. T.; Lodi, K. *J. Appl. Crystallogr.* **1997**, *30*, 744−749.
(30) Penfold, J.; Staples, E.; Lodhi, A. K.; Tucker, I.; Tiddy, G. J. T. *J. Phys. Chem. B* **1997**, 101.
(31) Zipfel, J.; Lindner, P.; Richtering, W. *Prog. Colloid Polym. Sci.* **1998**, *110*, 139−143.
(32) Lukaschek, M.; Muller, S.; Hansenhindl, A.; Grabowski, D. A.; Schmidt, C. *Colloid Polym. Sci.* **1995**, *274*, 1−7.
(33) Muller, S.; Borschig, C.; Gronski, W.; Schmidt, C.; Roux, D. *Langmuir* **1999**, *15*, 7558−7564.